THEORETICAL EVALUATION OF THE PERMEABILITY OF DISCHARGE ITEM (LiOOH) IN Li-O_2 BATTERIES

A.U. HASSAN† and C. GULERYUZ‡

† *University of Gujrat, Faculty of Science, Department of Chemistry, 50700 Gujrat, Pakistan*
hassanabrar2016@gmail.com
‡ *Marmara University, Faculty of Science and Arts, Department of Physics, Istanbul, 34000, Turkey*

***Abstract*— Both lithium ions and protons have been directly implicated in oxygen reduction and evolutionary responses and lithium hydroperoxide and lithium hydroxide are recognized as prevailing discharge ingredients. Attributes of lithium hydroperoxide shall be evaluated in principle. Impressively, the reaction of lithium hydroperoxide to triiodide shows quicker material properties, which allows a slightly lower excessive-potential during the charging cycle. The frontier molecular orbitals (FMOs), UV-Vis, and solvation model-based studies remained unknown. Therefore, we intended to study the Reaction path study, natural bond orbital, FMOs, UV-VIS, thermodynamic properties and medium influence on solvation energies, dipole moment, FT-IR and FT-Raman using polarizable continuum model (PCM) and density-based solvation model (SMD). The electronic properties of the molecule were calculated by M06-2X/6-31G (d,P) and B3LYP/6-31G (d,p) level of theories. Natural bond orbital discloses that the optimum stabilization energy managed to reach 39.64 kJ / mol, which is accountable for the extra stability of the compound. Based on materials impacts on FT-IR and FT-Raman intensities are identified in the understudy compound. Frequencies improved from gas to the solvent process.**

***Keywords*— Lithium hydroperoxide, DFT, FMO, UV-Vis, B3LYP/6-31G (d,p),**

I. INTRODUCTION

The endeavor of high-energy channels well beyond state-of-the-art Li-ion batteries has engendered a spike in detailed research of the lithium-air rechargeable batteries (Kim *et al.*, 2018) since it has the potential to achieve almost the same impact on energy density as those of the gasoline (Song *et al.*, 2016). In the past two decades, the market for rechargeable batteries has grown owing to their growing demand for use in households, factories, and automobiles (Hassan *et al.*, 2018). Using the most researched aprotic lithium-oxygen (Li-O_2) system, for example, the creation of insoluble and shielding lithium peroxide (Li_2O_2) during charging and discharging process gives rise to surface supersaturation and porous blocking up of the cathode materials resulting in low energy consumption and reduced capacity (Yoo *et al.*, 2014). Lithium hydroperoxide (LiOOH) has been identified as one of the prevailing discharge products, announcing distinct battery chemistry for moisture-contaminated Li-O_2 battery packs (Tan *et al.*, 2016). Lithium hydroperoxide is an inorganic compound of the LiOOH formula. Due to its outstanding function of LiOOH in Li-O2 batteries, a variety of DFT-based studies have been published. This is made up of lithium cation (Li^+) and hydrogen peroxide anion (HOO^-). The excitation of LiOOH is the strongest and LiOH is the lowest of oxidation. While the distinction is presumably focused on the colorimetry, the formulation of LiOOH, its interaction, and, more specifically, the presence of the compound in the Li-O_2 battery must be clearly defined and established (Nkungli *et al.*, 2015).

II. METHODS

Total calculations were rendered utilizing Gaussian 09 software kit 12 including density functional theory (DFT) at M06-2X/6-31 G (d, P) and B3LYP/6-31 G (d, p)/6-31 G (d) theoretical levels. Quantum mechanical calculations based on density functional theory (DFT) were undertaken to evaluate the intrinsic reaction path study of the LiOOH. Geometry modeling and frequency simulations have been conducted for the compound.

The thermodynamic characteristics and solvent-free energies were tested using their standard equations. It is worth noting that perhaps the solvation-free energy (ΔG^0 solv) is measured using a mixed cluster-continuum model. The gas-phase energy oscillations, like the density-based SMD solvent model, have been re-optimized to incorporate the solvent effect in oil. The dimethoxyethane static dielectric permittivity and the solvent radius were drawn from the comparison.

All input data were designed using Gauss View 5.0.16 Chemcraft, Gauss View 5.0, and Avogadro Program 18 to evaluate output information.

III. RESULTS AND DISCUSSION

Our research begins with the theoretical evaluation of the permeability of a discharge item (LiOOH) of the Li-O_2 batteries to oxidation by Li_2O_2 and LiOH reactions. Reactions to Li_2O_2 and LiOH in the Li-O2 battery has been confirmed as:

$$Li_2O_2 + H_2O \rightarrow LiOOH + LiOH \quad (1)$$

$$LiOH + H_2O_2 \rightarrow LiOOH + H_2O \quad (2)$$

In the presence of surplus water, both products are solid (Li *et al.*, 2020). Reactions are required in hydrated shape, LiOOH. H_2O and LiOH H_2O (Ren *et al.*, 2017). Interestingly, if not conveniently, both of them Reactions refer to the same product LiOH, asserting that this molecule could induce drying.

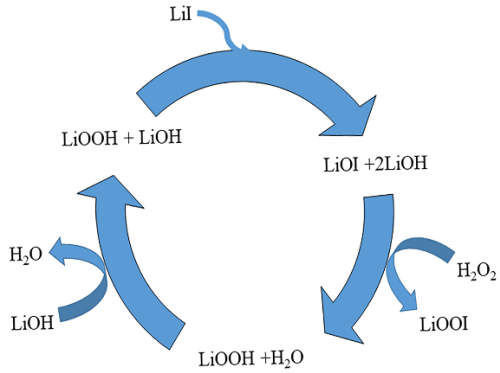

Fig. 1a. Schematic description of the fate of LiOOH during Li_2-O_2battery.

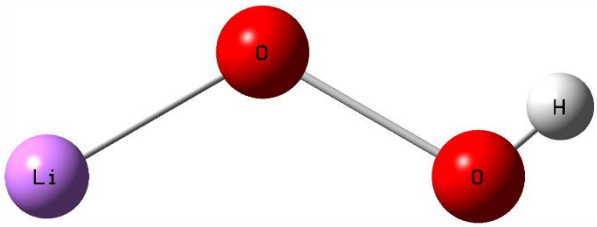

Fig. 1b. Optimized geometry of Lithium hydroperoxide (Li-OOH)

Identifying electronic influences that facilitate or impede the production of primary discharge/charge items or secondary intermediate is essential to the identification of the primary chemical reactions that can occur inside the population and the specific electrolytic media of the lithium-air battery (Kwak *et al.*, 2020).

The geometry of the compounds was optimized by using M06-2X (Glendening *et al.*, 2012)as well as B3LYP (Szafran and Katrusiak, 2007) levels of theory based on 6-31G(d, p). Nevertheless, the compound is also designed for B3LYP/6-31G(d) in the gaseous state and dimethyl sulfoxide as a solvent for the analysis of solvent effects over-optimized geometry(Ledesma *et al.*, 2009).

A. Molecular orbital analysis

Frontier molecular orbital theory has indeed been identified as the most exceptional theory for the elucidation of the chemical inertness of species (Wiesbrock and Schmidbaur, 2003). The highest occupied molecular orbital is represented by HOMO and the lowest unoccupied molecular orbital is represented by LUMO, which is regarded as a significant orbital of frontier molecular orbitals.

Typically, HOMO vitality shows the capacity to contribute an electron, but LUMO vitality refers to the potential to pick up an electron. The boundary orbital energy difference is a crucial feature to obtain information about the functional stability and chemical reactivity of the organisms (Janjua, 2018). The LiOOH orbital analysis was calculated using the M06-2X/6-31G(d, p) test. The computed energy of HOMO, LUMO, HOMO-1, LUMO+1, HOMO-2, LUMO+2 was approximately -0.18632,-0.05209, -0.21782, 0.01418,-0.27846 and 0.2307 a.u. Eventually, energy gaps such as $E_{HOMO–}E_{LUMO}$, $E_{HOMO-1–ELUMO+1}$, $E_{HOMO-2}–E_{LUMO+2}$ were identified as 0.249, 0.319, and 0.388, respectively. FMO energies are useful for determining global reactivity descriptors (Anguile *et al.*, 2018) including such global softness (S) (Mahmoud *et al.*, 2020), electron affinity (EA), ionization potential (IP), electron negativity (X), global hardness (Δ) (Anguile *et al.*, 2018), global electrophilicity index (ω) as well as the calibrated chemical potential (μ) using equations.

$$IP= -E_{HOMO} \quad (3)$$

$$EP= -E_{LUMO} \quad (4)$$

where IP determines the ionization potential (a.u), EA determines the electron affinity (a.u).

The chemical potential (μ), electro-negativity (χ), and chemical resilience were calculated using the theorem of Koopmans accompanying equations.

$$\chi = ([IP+EA])/2 = ([ELUMO + EHOMO])/2 \quad (5)$$

$$\eta = ([IP-EA])/2 = ([ELUMO-EHOMO])/2 \quad (6)$$

$$\chi = ([ELUMO + EHOMO])/2 \quad (7)$$

Global softness (σ) is characterized by the equation.

$$\sigma = 1/2\eta \quad (8)$$

The electrophilicity index has been implemented and from the following Equation.

$$\omega = \frac{\mu^2}{2\eta} \quad (9)$$

This metric was introduced to characterize the electrophilic intensity

The stability, specificity, and excitability of the species can be defined by global reactivity parameters. The most essential chemical feature is electronegativity (Prabhakara *et al.*, 2016), which defines the capacity of the species to draw electrons with itself. The global softness (S) of this molecule has been discovered to be 11.00, 2.380 and 3.125 Eh (Table 2).

This is 16 times more than the level of the general hardness (Δ). Such results indicated that this compound has lower toughness and higher softness values owing to the low energy difference between HOMO and LUMO. The softness factor means that the molecule may be chemically activated (Prakash and Malhotra, 2017). As a consequence, the bond interest quantities (when soft BV has used Parameters) of all atoms in the optimized configuration are similar to the predicted value contributing to a small GII 1⁄4 0.077 global instability index underpinning the plausibility of the structure model (Yang *et al.*, 2017)

B. FT-IR and FT-Raman analysis

The number of atoms with asymmetry point groups and effective vibratory normal modes was observed to be like that in the FT-IR as well as FT-Raman spectra

Table 1. Bonding Lengths (Å) as well as angles (°) Of LiOOH.

Bond length	Gas-phase	Solvent phase	Bond angles	Gas-phase	Solvent phase
R(1,2)	1.66	1.65	A(1,2,3)	120.0009	120.0005
R(2,3)	1.66	1.71	A(2,3,4)	109.4709	109.4500
R(3,4)	0.97	0.95	D(1,2,3,4)	180.0000	179.8970

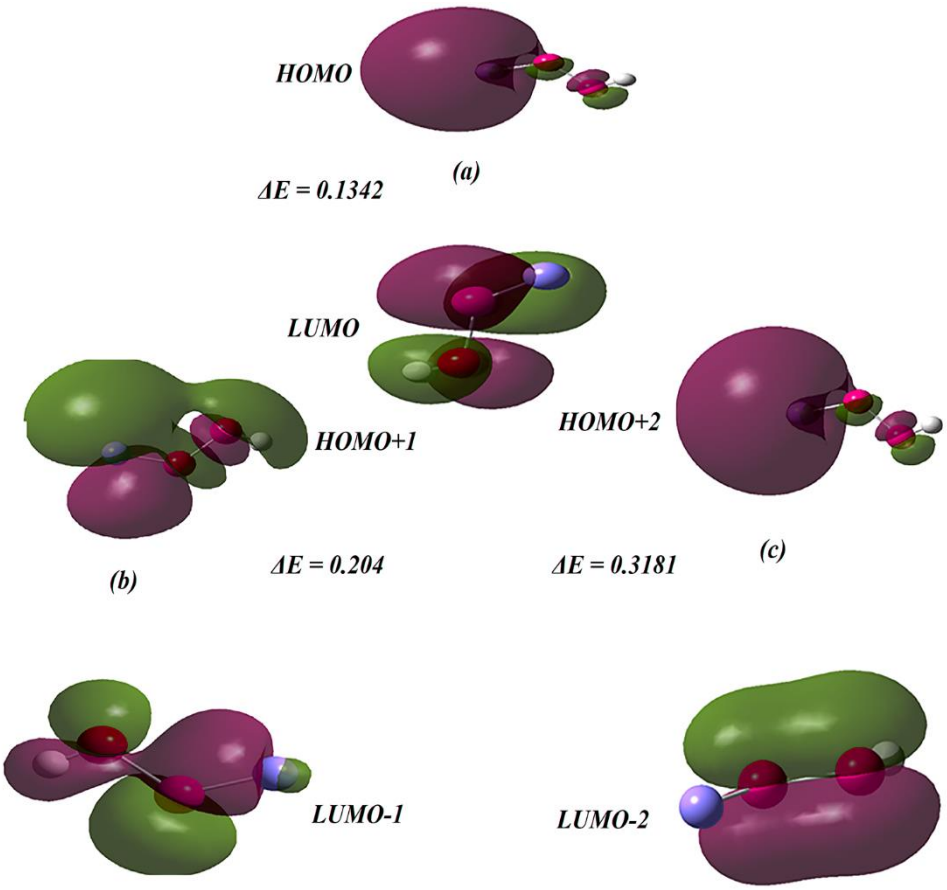

Fig. 2. Molecular orbital analysis of LiOOH at (a) HOMO-LUMO (b) HOMO+1- LUMO-1 and (c) HOMO+2- LUMO-2 .4

Table 2. Thermodynamic parameters of LiOOH

Parameter	**Molecular orbitals**		
	HOMO-LUMO	**HOMO-1-LUMO+1**	**HOMO-2-LUMO+2**
IP	-0.052	0.186	0.218
EA	-0.142	0.231	0.421
x	0.097	0.240	0.102
μ	-0.097	0.240	0.102
η	0.045	0.210	0.160
S	11.00	2.380	3.125
ω	0.104	0.137	0.033

Table 3 Optimized vibratory modes of LiOOH by tilizing B3LYP/6-31G(d)

Parameters	**Model number**					
	1	**2**	**3**	**4**	**5**	**6**
Frequency	336.67	100.39	441.84	898.430	1090.39	3786.36
FTIR	185.00	80.68	11.67	128.701	48.75	24.33
VCD*	0.00	0.00	-0.00	-0.003	-0.00	0.00
FT-Raman	5.52	3.38	23.17	18.539	7.96	143.77
Dipolar-P	0.75	0.31	0.35	0.29	0.69	0.27
Depolar-U	0.86	0.47	0.52	0.45	0.82	0.42

(Marchewka, 2002). The modes FT-IR and FT-Raman of the LiOOH hydroxyl group (OH) were positioned at 3418, 1456, and 896 (Marchewka, 2002). The vibratory frequency for O-H is centered at 3897 and also is allocated to it. Raman intensity levels were observed to be greater than FT-IR levels of intensity in the above-mentioned vibrational frequencies (Table 3). The Raman spectrum demonstrated a unique characteristic peak at about 860 cm, designated to the stretching of the O-O bond based on the Density Functional Theory (DFT) computations. Other fingerprint peaks for LiOOH were also noted at 80–150 cm (Fig. 3).

C. Reaction path study

Many of the unresolved questions in the elucidation of secondary structure components are how the atoms determine the right structure on a rational time scale (Jain and Mishra, 2016). It is believed that random searches through all possible configurations are just too slow and

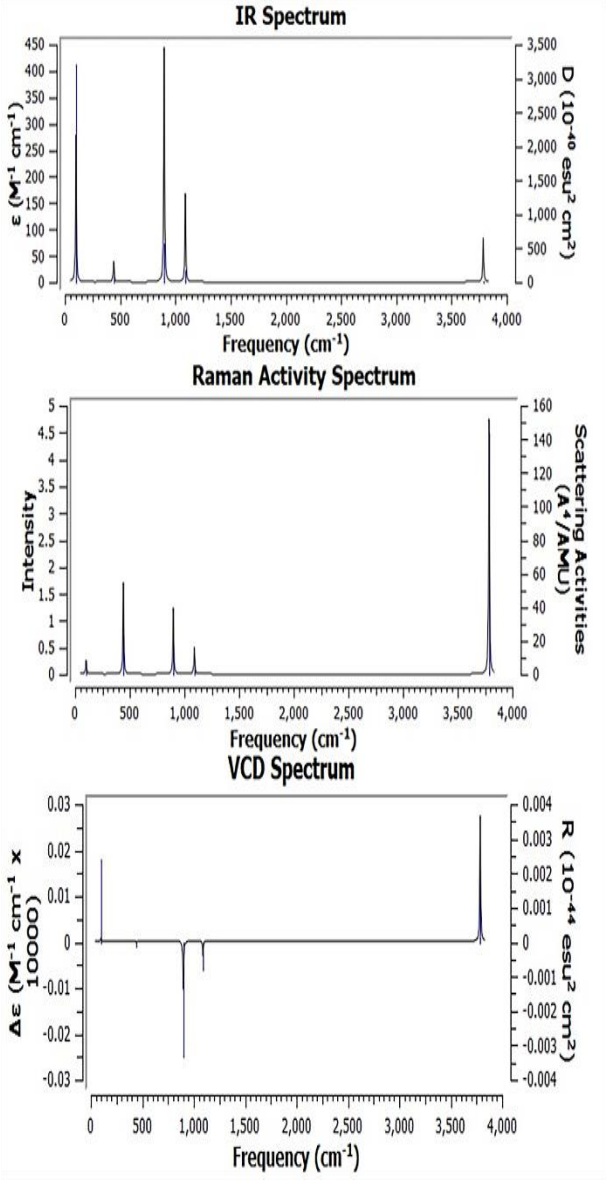

Fig. 3. Theoretical spectra of LiOOH

that some stable intermediates are biasing the actual foldable mechanism (Torres and Balbuena, 2018). Comprehensive microscopic simulations of the dynamics of crystal structures creation are not yet practicable (Kwak *et al.*, 2020). Even so, research of simpler model systems is being published previously, striving at formative construct into transcriptional activation in atomic skeletons (Czerminski and Elber, 1989). Detailed microscopic computations of the mechanics of secondary structural properties are not yet viable. The peroxide anion is a powerful nucleophile and is quite large. The O−O bond dissociative indications of dissociation energy are 47 kcal/mol equivalent to 118 kcal/mol. The computed reaction route for LiOOH in the gaseous state and with an apparent solvent (dimethoxyethane) is shown in Fig. 4. It should be remembered that Li is seen in the first stages of the reaction process since it was used to calculate the relative energy and to answer to the chemical reaction (Czerminski and Elber, 1989).

IV. CONCLUSIONS

In the present study, the basic chemical encounters that assist to justify the innovative ingredients identified in the electrolyte solution media of the Li-O2 battery have been studied theoretically. The resulting reaction to recycle oxygen is unaffordable based on the experimental findings collected. The current study also shows that the optimized bond lengths and bond angles demonstrate excellent communications with the X-ray and DFT data published. The catalytic impact of iodide in the peroxide bond depolarization is seen to be possible owing to the halogen-bond association here between iodine atom and the oxygen nucleophilic site contributing to the O−O bond deformation. FT-IR and Raman's frequencies have increased in comparison to recorded values in all approaches, but good continuity has been developed between the processes investigated.

REFERENCES

Anguile, J.J., Ngnabeuye O.N., Bridget, N.N., Fomuta, T.R., Djoumbissie, A.L., Tagne, A.C.K. and Ngoune, J. (2018) Synthesis, Characterization and DFT Studies of Two Zinc(II) Complexes Based on 2-Isopropylimidazole. *Open Journal of Inorganic Chemistry*. **8**, 105–124.

Czerminski, R. and Elber, R. (1989) Reaction path study of conformational transitions and helix formation in a tetrapeptide. *Proceedings of the National Academy of Sciences of the United States of America*. **86**, 6963–6967.

Glendening, E. D., Landis, C. R. and Weinhold, F. (2012) Natural bond orbital methods. *Wiley Interdisciplinary Reviews: Computational Molecular Science*. **2**, 1–42.

Hassan, A.U., Mohyuddin, A. and Ali, S. (2018) Preparation of rechargeable battery from poultry waste. *Pakistan Journal of Scientific and Industrial Research Series A: Physical Sciences*. **61**, 80–83.

Jain, R.K., and Mishra, A.P. (2016) Microwave synthesis, spectral, thermal, 3D molecular modeling analysis and antimicrobial activities of some transition metal complexes of Schiff bases derived from 5-bromosalicylaldehyde, *Journal of Saudi Chemical Society*. **20**, 127–137.

Janjua, M.R.S.A. (2018) Structural Properties and Nonlinear Optical Responses of Halogenated Compounds : A DFT Investigation on Molecular Modelling. *Open Chem.* **16,** 978–985.

Kim, M.-C., So, J.-Y., Moon, S.-H., Han, S.-B., Choi, S., Kim, E.-S., Shin, Y.-K., Lee, J.-E., Kwak, D.-H., Bae, W.G. and Park, K.-W. (2018) Nature-inspired cathodes using high-density carbon papers with an eddy current effect for high-rate performance lithium-air batteries. *Journal of Materials Chemistry A*. **6**, 9550–9560.

Kwak, W.-J., Chae, S., Feng, R., Gao, P., Read, J., Engelhard, M.H., Zhong, L., Xu, W. and Zhang, J.-G. (2020) Optimized Electrolyte with High Electrochemical Stability and Oxygen Solubility for Lithium–Oxygen, and Lithium-Air Batteries. *ACS Energy Letters*. **5,** 2182–2190.

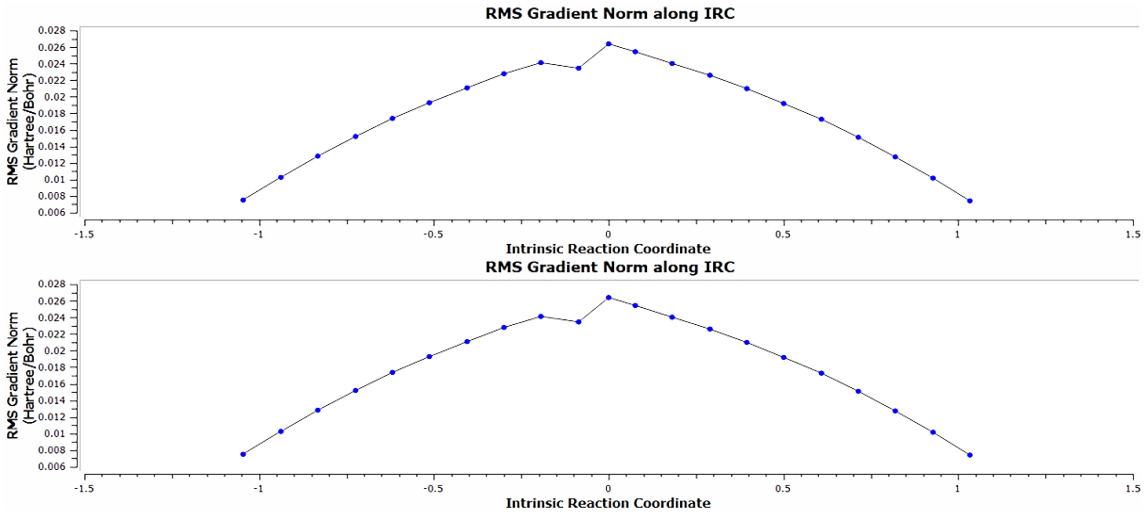

Figure 4. Intrinsic Reaction (IRC) Path study of LiOOH

Ledesma, A.E., Zinczuk, J., Altabef, A.B., López González, J.J. and Brandán, S.A. (2009) Synthesis and vibrational analysis of N-(2′-furyl)-imidazole. *Journal of Raman Spectroscopy*. **40**, 1004–1010.

Li. D., Zhang, S., Zhang, Q., Kaghazchi, P., Qi, H., Liu, J. Guo, Z., Wang, L. and Wang, Y. (2020) Pencil-drawing on nitrogen and sulfur co-doped carbon paper: An effective and stable host to pre-store Li for high-performance lithium-air batteries. *Energy Storage Materials*. **26**, 593–603.

Mahmoud, W.H., Deghadi, R.G. and Mohamed, G.G. (2020) Cyclometalated complexes containing ferrocenyl Schiff base: Preparation, characterization, DFT calculations, application in cancer and biological researches and MOE studies. *Arabian Journal of Chemistry*. **13**, 5390–5405.

Marchewka, M.K. (2002) Infrared and Raman spectra of aluminum chloride hemihydrate. *Materials Science and Engineering B: Solid-State Materials for Advanced Technology*. **95**, 214–221.

Nkungli, N.K., Ghogomu, J.N., Nogheu, L.N. and Gadre, S.R. (2015) DFT and TD-DFT Study of Bis[2-(5-Amino-[1,3,4]-Oxadiazol-2-yl) Phenol] (Diaqua) M(II) Complexes [M = Cu, Ni, and Zn]: Electronic Structures, Properties, and Analyses. *Computational Chemistry*. **3**, 29–44.

Prabhakara, C.T., Patil, S.A., Toragalmath, S.S., Kinnal, S.M. and Badami, P.S. (2016) Synthesis, characterization and biological approach of metal chelates of some first-row transition metal ions with halogenated bidentate coumarin Schiff bases containing N and O donor atoms, *Journal of Photochemistry and Photobiology B: Biology*. **157**, 1–14.

Prakash, A. and Malhotra, A.P.R. (2017) Co (II), Ni (II), Cu (II) and Zn (II) complexes of aminothiazole - derived Schiff base ligands: Synthesis, characteriza-tion, antibacterial and cytotoxicity evaluation, bovine serum albumin binding and density functional theory studies. *Applied Organometallic Chemistry*. **32,** e4098.

Ren, X., Liao, B., Li, Y., Zhang, P., Deng, L. and Gao, Y., (2017) Facile synthesis of PdSnCo/nitrogen-doped reduced graphene as a highly active catalyst for lithium-air batteries. *Electrochimica Acta*. **228**, 36–44.

Song, Y.-M., Kim, C.-K., Ki, K.-E. Hong, S.Y. and Choi, N.,S. (2016) Exploiting chemically and electrochemically reactive phosphite derivatives for high-voltage spinel $LiNi_{0.5}Mn_{1.5}O_4$ cathodes. *Journal of Power Sources*. **302**, 22–30.

Szafran, M. and Katrusiak, A. (2007) Hydrogen bonds and electrostatic interactions in 1 : 1 and 2 : 1 complex of homarine with mineral acids studied by NMR, FTIR, DFT and X-ray diffraction. **827**, 56–66.

Tan, P., Wei, Z.H., Shyy, W., Zhao, T.S. and Zhu, X.B. (2016) A nano-structured RuO_2/NiO cathode enables the operation of non-aqueous lithium-air batteries in ambient air. *Energy and Environmental Science*. **9**, 1783–1793.

Torres, A.E., and Balbuena, P.B. (2018) Exploring the LiOH Formation Reaction Mechanism in Lithium-Air Batteries. *Chemistry of Materials*. **30**, 708–717.

Wiesbrock, F. and Schmidbaur, H. (2003) Complexity of coordinative bonding in thallium(I) anthranilates and salicylates. *Journal of the American Chemical Society*. **125**, 3622–3630.

Yang, J., Ma, D., Li, Y., Zhang, P., Mi, H., Deng, L., Sun, L. and Ren, X. Atomic layer deposition of amorphous oxygen-deficient TiO_{2-x} on carbon nanotubes as cathode materials for lithium-air batteries. *Journal of Power Sources*. **360**, 215–220.

Yoo, H.D., Markevich, E., Salitra, G., Sharon, D. and Aurbach, D. (2014) On the challenge of developing advanced technologies for electrochemical energy storage and conversion. *Materials Today*. **17**, 110–121.

Received: June 25, 2020
Sent to Subject Editor: July 7, 2020
Accepted: March 28, 2021
Recommended by Subject Editor María Luján Ferreira